RESEARCH PAPER

Advanced Brain Tumor Classification Utilizing Multi-Anchor Space-Aware Temporal Convolutional Neural Network Integrated With Distributedsupport Vector Machines For Accurate MRI Image Analysis.

R . Sankaranarayanan[1*], S.K. Susee[2] ,M. Senthil Kumar[3], B. Chidhambara Rajan[4]

[1*]*Assistant Professor University: NIMS University Rajasthan, Jaipur Email ID: sankarnba22@gmail.com*
Orcid ID:http://orcid.org/0000-0002-6918-0594
[2]*Assistant Professor University: Mohamed Sathak A.J. College of Engineering Email ID: suseekannan07@gmail.com*
Orcid ID:http://orcid.org/0009-0009-6277-7724
[3]*Professor University: Karpaga Vinayaga College of Engineering and Technology Email ID: msen1982@gmail.com*
Orcid ID:http://orcid.org/0000-0002-7158-8898
[4]*Professor University: SRM Valliammai Engineering College Email ID: profbcr@yahoo.com*
Orcid ID:http://orcid.org/0000-0003-

ABSTRACT
Brain tumors (BT) remain a major clinical challenge due to their heterogeneous structure, complex morphology, and limited therapeutic efficacy caused by variability in drug penetration across tumor sub-regions. Accurate characterization of tumor tissues is therefore essential not only for diagnosis but also for optimizing targeted drug delivery, treatment planning, and therapeutic decision-making. In this study, an AI-assisted MRI-based brain tumor characterization framework, termed BTC-MSTCNN-DSVM-MRI, is proposed to support pharmaceutical and therapeutic planning. MRI images obtained from the BRATS 2020 dataset are pre-processed using a Switching Model Stein Variational Sampling Filter (SMSVSF) to perform resizing, normalization, and noise reduction. Data augmentation techniques, including rotation, flipping, and scaling, are applied to enhance dataset diversity and model generalization. A Multi-Anchor Space-Aware Temporal Convolutional Neural Network (MSTCNN) is employed to extract intensity-based, shape-based, and texture features from MRI images, capturing spatial and temporal tumor heterogeneity. These features are classified using Distributed Support Vector Machines (DSVM) to accurately characterize tumor sub-regions into GD-enhancing tumor, peritumoral edema, necrotic tissue, and non-enhancing tumor core, which are clinically relevant for drug delivery optimization. Furthermore, a Super Cell Thunderstorm Algorithm (STA) is utilized to optimize model parameters, improving classification reliability and computational efficiency. Experimental results demonstrate superior performance with an accuracy of 99.55%, precision of 98.75%, and recall of 98.65%, outperforming existing state-of-the-art methods. The proposed framework provides a robust decision-support tool for targeted drug delivery and personalized brain tumor therapy..
Keywords: Brain tumor; MRI; Drug delivery; Therapeutic planning; Deep learning; Pharmaceutical decision support
How to cite this article: Sankaranarayanan R, Susee SK, Senthil Kumar M, Chidhambara Rajan B.. Advanced Brain Tumor Classification Utilizing Multi-Anchor Space-Aware Temporal Convolutional Neural Network Integrated With Distributedsupport Vector Machines For Accurate MRI Image Analysis...Int J Drug Deliv Technol. 2026;16(2s): 990-1008; DOI: 10.25258/ijddt.16. 990-1008
Source of support: Nil.
Conflict of interest: None

INTRODUCTION

The rising incidence of BT in patients poses a important danger to the health industry due to factors such as disease complexity and high mortality rates [1, 2]. The identification of an issue is precise and fast to aid in the development of various treatment processes useful to patients [3, 5]. Magnetic resonance imaging (MRI) is a crucial tool not only for identifying brain tumors but also for guiding drug delivery strategies by visualizing tumor heterogeneity and tissue characteristics [6]. However, the procedure of manual segmentation is labour-intensive and associated with tiny changes between the different observers, therefore there is a need to develop more automatic and reproducible diagnostic techniques [7, 9]. Advancements in neural networks can be employed in neural networks for automating the brain tumors categorization [10, 14]. Deep neural systems, such as Convolutional Neural Networks (CNN) is used for image analysis owing to their capability to handle raw data and extract significant information from it. CNNs have expanded their use in two important areas of medical image analysis: cancer detection and categorization [15]. CNN, like many other predictive models, are prone to overfitting when trained on limited datasets, and struggle to generalize to new data.SVMs, also known as supervised learning approaches, are common linear classification algorithms that have proven to be effective, particularly when dealing with small data sets [16]. Such models can perform well with high-dimensional features and generalize effectively if the correct parameter values are tuned.However, it has been noted that the quality of the characteristics provided to them has a significant impact on their performance [17]. This research proposes a new

**Author for Correspondence: sankarnba22@gmail.com*

hypothesis that merges CNNs and SVMs to improve MRI-based tumor characterization, thereby supporting optimized drug delivery, treatment stratification, and pharmacological decision-making. This indicates that the proposed technique takes full advantage of neural network approaches in feature extraction by CNN while remaining strong in classification via SVM [18]. This fusion technique is designed with respect to the integration of numerous limitations that arise when the above-mentioned classification of processes is conducted independently, with the objective of increasing both the exactness and believability of brain tumor diagnosis [19, 20].

Brain tumor diagnosis and classification remain difficult due to differences in tumor shape, size, and location, which frequently result in diagnostic mistakes. Typical imaging methods usually have difficulties in identifying small or complicated abnormalities and this restricts their therapeutic application. The lack of specific and computerized procedures makes the diagnosis of the patients to be postponed and their survival to be reduced. The solution to these challenges and enhancements to tumor detection and classification is a strong and highly precise analytical method. The above disadvantages have inspired the development of an effective way of identifying brain tumors using MRI.

A novel approach for brain tumor categorization uses an MSTCNN to extract intensity, shape, and texture information from MRI images, capturing both spatial and temporal fluctuations in tumor formations. The collected features are identified using DSVM, which ensures accurate categorization of various tumor types. STA optimization improves classification precision while reducing computational complexity and allowing for more reliable early tumor identification than existing approaches. Accurate identification of tumor sub-regions plays a vital role in pharmaceutical science, as drug penetration, therapeutic efficacy, and toxicity vary significantly across enhancing, necrotic, and edematous tumor tissues. MRI-guided tumor characterization therefore serves as an essential decision-support tool for selecting appropriate drug delivery routes, dosage levels, and treatment modalities.

The key contributions of this manuscript;

- The objective of this research is to create an optimized hybrid MSTCNN-DSVM framework for accurate and effectual brain tumors categorization of from MRI imageries.
- SMSVSF is used for effectual image resizing, normalization, noise reduction, together with augmentation approaches rotation, flipping, scaling to boost dataset variety.
- MSTCNN was developed to extract intensity-based, shape-based and texture data from MRI imageries for detailed representation of tumor characteristics.
- The extracted features are loaded into DSVM, which accurately categorize tumors as GD-enhancing tumor, peritumoral edema, necrotic tissue, non-enhancing tumor core.
- The STA is developed to optimize MSTCNN-DSVM settings, improving categorization reliability while minimizing computing complexity.

Following portions of this work are structured as below: part 2 presents literature survey, part 3 explains proposed methodology, part 4 demonstrates outcome and part 5 gives conclusion.

2. Literature Survey

A lot of works were suggested in literature based on deep learning dependent MRI brain tumor detection; some of recent works are revealed below,

In 2024, Yurtsever, M.E., et al., [21] have introduced a development of brain tumor radio genomic categorization with GAN-dependent augmentation of MRI slices in the newly released gazi brains dataset. It aims to improve deep learning (DL) model performance by enhancing brain MRI slices. To avoid any leakage, augmentation is only performed to training data. StyleGanv2-ADA technique was trained on Gazi Brains 2020, BRaTS 2021, Br35h datasets with researchers' default settings. The suggested strategy improves the accuracy of brain tumor categorization models on Gazi Brains 2020, BraTS 2021, Br35h. It provides high recall and low accuracy.

In 2024, Preetha, R., et al., [22] have presented a fine-tuned EfficientNet-B4 Convolutional Neural Network for the automated BT detection from MRI. Using EfficientNet-B4 as the basic model and programmable layers, it offers a novel method for detecting brain tumours utilizing deep convolutional neural networks. The model conducted an ablation research to assess the effect of various components on performance, such as layer alterations, batch size changes, optimizers, loss functions, and learning rates. The research identified the ideal configuration, improving the model's robustness, reliability in classification. It provides high precision and low recall.

In 2024, Pacal, I., et al., [23] have introduced an enhancing EfficientNetv2 with global and effectual channel attention mechanisms for appropriate MRI-dependent brain tumor categorization. To overcome these issues, it introduces a new version of EfficientNetv2 architecture which is a combination of Efficient Channel Attention and Global Attention Mechanism (GAM). This modification greatly improves the accuracy of the brain tumour classification besides increasing the ability of the methods to bring out important features in complicated MRI images. The presented method was unique and more effective in identifying a variety of brain tumours because it meticulously incorporates attention mechanisms that systematically enhance feature extraction. It attains greater recall and lesser accuracy.

In 2024, Nassar, S.E., et al., [24] have introduced a reliable hybrid deep learning method for categorizing brain tumours based on MRI. Because of the gravity and sensitivity of the challenges involved, biomedical engineering recognizes the significance of this remarkable accomplishment. Because deep learning has

a remarkable ability to handle large amounts of data without human error, its application to the identification and categorization of BT in particular and malignancies in general using MRI was crucial for speed and accuracy. To help radiologists avoid wasting time examining at multiple images to get an accurate diagnosis, the suggested study aimed to provide an effective automated system for categorising brain tumours. It attains greater F1-score and lesser precision.

In 2024, Joshi, A.A. and Aziz, R.M., [25] have presented a deep learning method that uses gene expression data and metaheuristic optimisation to classify brain tumours. It presents a brand-new optimisation technique called PSCS, which blends deep learning and the BT categorization. PSCS uses the Cuckoo Search method to improve Particle Swarm Optimisation exploitation. Then, using PSCS optimisation technique and Deep Learning (DL) to detect different groups or classes connected with a certain tumour, gene expression data of brain tumours were identified. It attains greater precision and lesser recall.

In 2024, Simo, et al., [26] have presented performance by implementing deep learning technique for categorizing brain tumours from MRI data. The presented study develops a deep learning and fully CNN-based sequential BT detection and categorization model. The suggested approach consists of two steps: discriminating among non-neoplastic and neoplastic brain, defining tumor type of latter. The Brain Tumour MRI Dataset was utilized for training two techniques. To attain the best findings, Adam, Nesterov momentum, root-mean-square propagation, adaptive gradient were explored. It provides high precision and low F1-score.

In 2024, Malakouti, S.M., et al., [27] have introduced machine learning and transfer learning methods for appropriate BT categorization. It classifies healthy and ill individuals using MRI pictures and numerical data using ML and transfer learning techniques. Light Gradient Boosting Machin, AdaBoost, gradient boosting, Random Forest, logistic regression, quadratic discriminant analysis, linear discriminant analysis, other transfer learning techniques were combined with 3762 MRI data. LightGBM was used to process numerical data, and it achieved a reliability of ninety-five percent. Transfer learning was used in image data using modified GoogLeNet model increased the success rate of classification to ninety-nine percent. It achieves greater recall and lesser accuracy. Table 1 represents comparison of literature survey

Table 1: Comparison of Literature Survey

Author	Models	Objectives	Merits	Demerits
Yurtsever et al., [21]	GAN-based augmentation and Radio genomic classification	Enhance brain tumor classification using augmented MRI slices	Increases dataset diversity, improves robustness	GAN may introduce synthetic artifacts, high computational cost
Preetha et al., [22]	Fine-tuned EfficientNet-B4	Automated brain tumor detection from MRI	High accuracy, efficient feature extraction	May over fit on small datasets, needs careful tuning
Pacal et al., [23]	EfficientNetv2 Global & Efficient Channel Attention	Accurate MRI-dependent brain tumor categorization	Improves feature attention, enhances classification accuracy	Complex architecture, higher computational requirement
Nassar et al., [24]	Hybrid deep learning	Robust MRI-dependent brain tumor categorization	Combines multiple models for better performance	Increased training complexity, requires large dataset
Joshi & Aziz [25]	Deep learning and Metaheuristic optimization	Brain tumor classification using gene expression data	Optimizes feature selection, improves predictive performance	Metaheuristic optimization is time-consuming, complex
Simo et al., [26]	Deep learning CNN	Improve brain tumor categorization	Simple end-to-end framework, good performance	May need large annotated datasets, lacks interpretability
Malakouti et al., [27]	ML and Transfer learning	Accurate brain tumor categorization	Leverages pre-trained models, reduces training time	May underperform on domain-specific MRI data

Table 1 represents comparison of literature survey. Despite substantial progress in BT categorization utilizing deep learning, transfer learning, hybrid methods, major research gaps remain. Most existing research relies largely on large, high-quality annotated MRI datasets, which limits their generalizability to smaller or diverse datasets. GAN-based augmentation and metaheuristic optimization boost performance while increasing computing complexity and potential artifacts. Moreover, most models, especially deep learning and transfer learning models cannot be interpreted, which complicates their clinical implementation. Attention techniques and mixed models enhance accuracy and complexity of architecture, which can be a hindrance to real time applications. In order to allow successful clinical application, models balances high accuracy, computational efficiency, small or noisy data robustness, and interpretability.

3. Proposed Methodology

This part talks about proposed BTC-MSTCNN-DSVM-MRI to detect and classify BT directly out of MRI imageries to improve the precision of the diagnosis and the efficiency of the computation. This procedure consists of six key phases, namely, Data Collection, Pre-processing, Data Augmentation, Feature Extraction, Classification, Optimization. Initially, MRI images are gathered from BRATS 2020 dataset. Pre-processing is performed using the **SMSVSF** to resize, normalize, and reduce noise in the images. To improve dataset variability and strengthen generalization, augmentation techniques like rotation, flipping, scaling are applied. The pre-processed imageries are supplied into **MSTCNN,** which extracts intensity-based, shape-based and texture features. These features are classified by the **DSVM** into GD-enhancing tumor, peritumoral edema, necrotic tissue, non-enhancing tumor core. Finally, the **STA** is used to improve the MSTCNN-DSVM parameters, ensuring improved classification performance and reduced computational complexity. Figure 1 depicts block diagram of proposed BTC-MSTCNN-DSVM-MRI methodology and comprehensive description of every stage is described below.

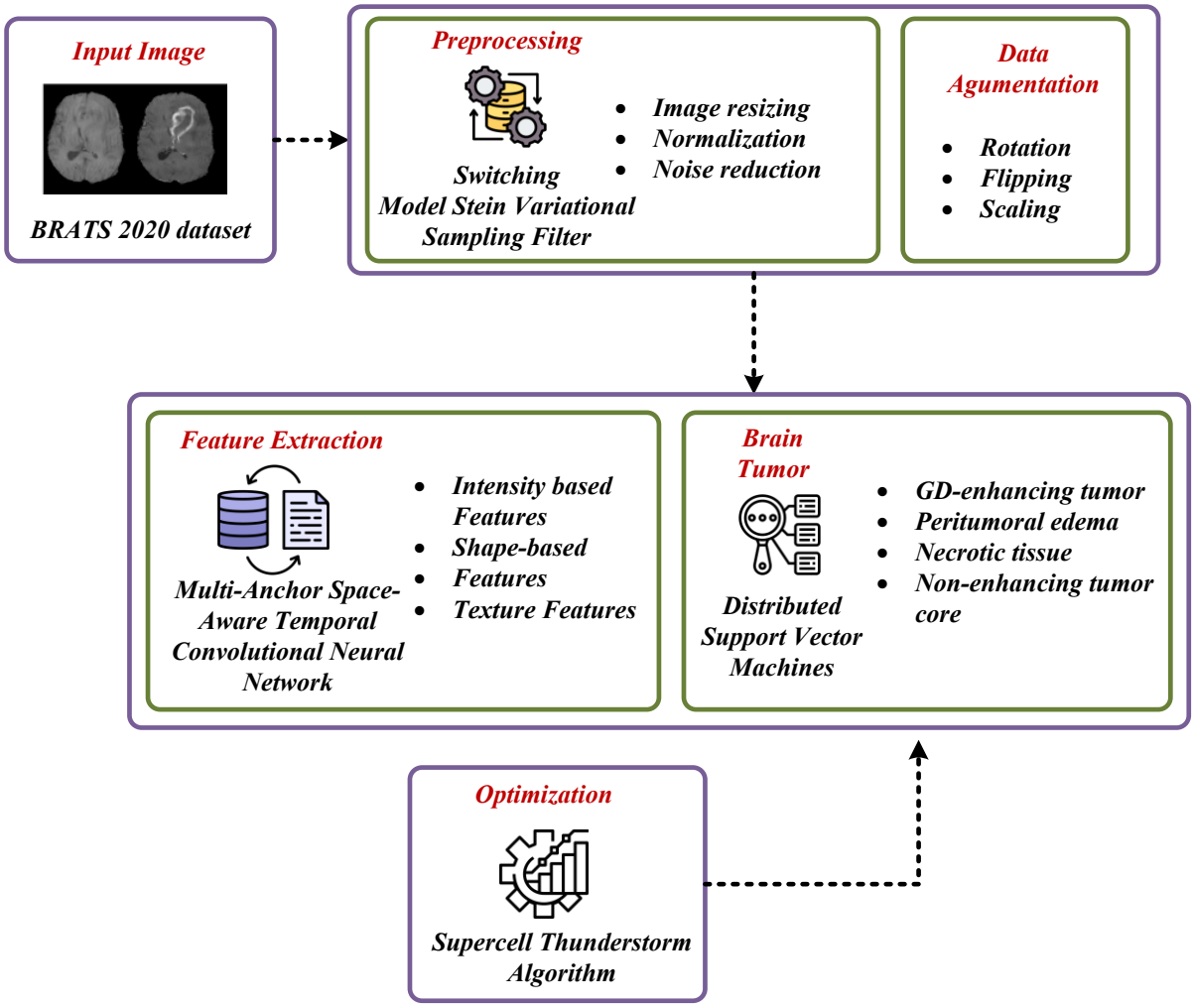

Figure 1: Block diagram of the BTC-MSTCNN-DSVM-MRI technique

3.1 Image Acquisition

In this section, image is collected from BRATS 2020 dataset [28]. The BraTS 2020 dataset is an extensive collection of multi-institutional, pre-operative multimodal MRI scans, including 369 glioma cases for training, 125 for validation, 166 for testing, which account for about 58.6%, 19.8%, and 26.4% of the dataset, respectively. Each subject comprises four MRI modalities (T1, T1ce, T2, FLAIR) that have been standardized to a common atlas and voxel resolution, as well as expert-annotated segmentations of three tumor sub regions enhancing tumor, necrotic core, peritumoral edema for training set. The validation set evaluates models on unseen data without ground-truth labels, whereas the test set is saved for the ultimate task evaluation. This dataset serves as a standard for brain tumor characterization for drug delivery and therapeutic planning, overall survival forecasting, and uncertainty quantification, enabling the creation and evaluation of automated medical imaging algorithms based on commonly accepted metrics such as Dice coefficient and accuracy. Its widespread application and uniform format make it an essential resource for developing brain tumor analysis in medical imaging analysis. Figure 2 shows Sample Images of BRATS 2020 dataset and Table 2 represents the Percentage distribution of number of MRI samples.

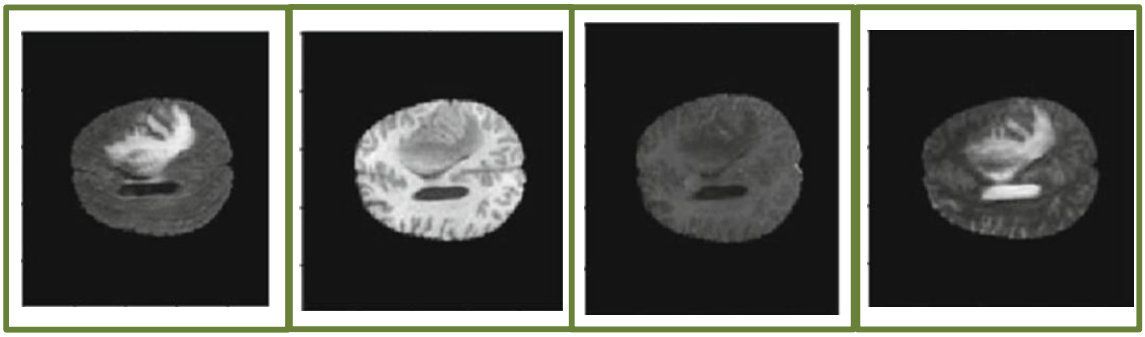

Figure 2: Sample Images of BRATS 2020 dataset

Table 2: Percentage distribution of number of MRI samples

MRI Modality	Number of Samples
T1	500
T2	500
FLAIR	500
T1Gd	500
T1	500

Table 2 displays percentage distribution of MRI samples depending on the suggested modalities in BRATS 2020 dataset. Each of the different modalities contains 500 samples, thus the total count of MRI scans utilized is 2000. The data's wide and reasonably standard nature makes it acceptable for use in the categorization of brain tumors in research investigations.

3.2 Enhanced Image Processing through Switching Model Stein Variational Sampling Filter

In this section, Preprocessing using (SMSVSF) [29] is discussed. SMSVSF is used for image resizing, normalization, noise reduction. The use of the SMSVSF in Preprocessing hasvarious advantages. It effectively handles image resizing, normalization, noise reduction ensuring that MRI scans are standardized for further analysis. SMSVSF maintains important structural details of brain tissues while minimizing random noise and artifacts which improves the clarity of tumor boundaries. This enhances the quality, consistency , reliability of input data, reduces computational errors during feature extraction and improves the performance and accuracy of brain tumor categorization methods. Multiple sampling particles are initialized to represent diverse possible image states, ensuring robust estimation as given in equation (1).

$$x\left(z_t, k_t \middle| z_{1:t-1}, k_{1:t-1}, m_{1:t}\right) \quad (1)$$

Here x implies raw input image; k_t implies Kernel function; z_t represents the resized to a fixed dimension; $z_{1:t-1}$ represents the initial random variable; $m_{1:t}$ implies standardization is crucial for techniques that need uniform input dimensions. The filter adaptively switches between model states according to image characteristics. Thus, it is given in equation (2).Figure 3 represents Sample pre-processed images from BRATS 2020 dataset.

$$\alpha_{zt}\log y\left(z_t,k_t\left|z_t^{(j)}\right.\right)=\alpha_{zt}\log y\left(z_t,k_t\left|zj\right.\right)+\alpha_{zt}\log y\left(z_z\left|z_{z-1}\right.\right) \quad (2)$$

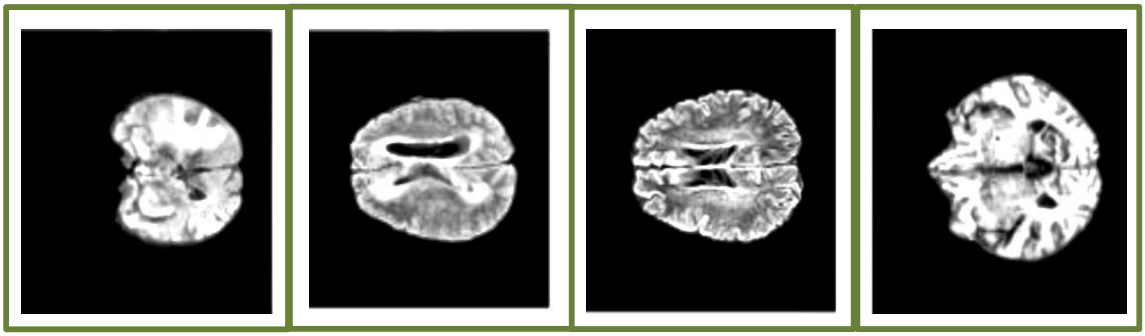

Figure 3: Sample pre-processed images from the BRATS 2020 dataset

Where α_{zt} represents the iterative sampling process; $\log y$ represents the possible sample of the image state; $z_t^{(j)}$ represents the total number of model states. Particles are updated via stein variational gradient descent moving them toward the optimal distribution while preserving diversity as given in equation (3).

$$\alpha_{zt}\log y\left(z_t,k_t\left|z_t^{(j)}\right.\right)\frac{\alpha_{zt}\log y\left(z_t,k_t\left|z_t^{(j)}\right.\right)}{\left\|\alpha_{zt}\log y\left(z_t,k_t\left|z_t^{(j)}\right.\right)\right\|} \quad (3)$$

Where α represents update computed from the gradient of the target distribution; z represents the current state or mode of the system; y denotes the possible image state. Random noise and MRI artifacts are suppressed while preserving fine structural details of brain tissue and tumor regions. Thus, it is given in equation (4).

$$z\left(y_t^{(j)},k_t^{(j)}\left|q_{1:t}^{(k)},k_{1:z-1}^{(k)}\right.\right)=\partial\left(g_z^{(j)}\right)k\left(u_z^{(j)}\right)\left(y_z^{(j)}\right) \quad (4)$$

Where $q_{1:t}^{(k)}$ represents the denoising and artifacts removal process; ∂ represents the tumor regions and $u_z^{(j)}$ represents the brain tissue. Intensity values are normalized to a consistent scale to reduce variability and imageries are resized to uniform dimensions for feature extraction and classification as given in equation (5).

$$x\left(K_m.h_m+F_k.N_m.h_k+\left(F_k.-N_m.\right).g_\alpha\right) \quad (5)$$

Where x implies resized uniform dimensions; K_m implies handling of varying noise patterns and image characteristics; $F_k.$ represents the enhance image quality; g_α represents the noise reduced.

3.2.1 Data Augmentation

The authors added that training with additional data using a variety of data augmentation techniques was necessary due to the relatively limited sample. The transformation planes were scaled, mirrored, arbitrarily rotated, and given Gaussian noise, to name a few of the distortions are previously applied. To promote training variety and decrease the probability of situations that lead to in overfitting, augmentation often helps to enhance the range of the training set.

Rotation:The process of applying rotation to images taken by MRI involves turning them at random degrees, 90°, or 180°. This simulates variances in the real environment by assisting the model in identifying tumors in various orientations. For categorization tasks, it enhances generalization and lessens orientation bias.

Flipping: Flipping is the process of creating mirror versions of an image by reversing it either vertically or horizontally. Without changing the significance of the tumor structure, this creates fresh perspectives on it. It guarantees that the model picks up symmetry patterns and becomes more resilient to changes in position.

Scaling: Scaling zooms in or out of the MRI image while maintaining proportions to change its size. By simulating tumors of different sizes and distances, this improves the accuracy of detection. It guarantees that the model can withstand variations in magnification and resolution.A sample image of data augmentation is represented in Figure 4.

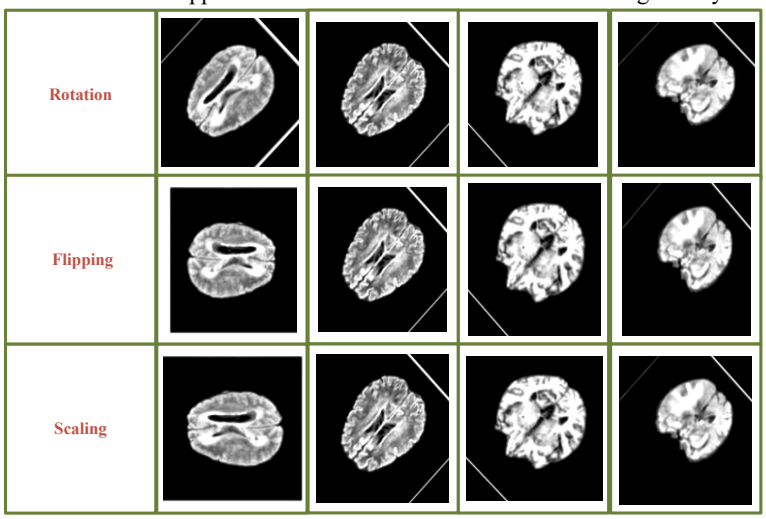

Figure 4: SampleImage of Data Augmentation

Finally, SMSVSF has successfully image resized, normalized and noise reduced. The pre-processing output is supplied to feature extraction.

3.3 Brain Tumor Classification utilizing Multi-Anchor Space-Aware Temporal Convolutional Neural Network Integrated with Distributed Support Vector Machines

The proposed MSTCNN-DSVM is used to enhance diagnostic accuracy. MSTCNN extracts mentioned features from pre-processed MRI images using multi-anchor convolutional layers that capture local and global contextual information, followed by space-aware temporal layers for dynamic feature representation. These extracted features are fused and provided into DSVM, which performs robust classification into tumor subtypes, ensuring precise and efficient detection. Figure 5 shows the Architecture Diagram of MSTCNN-DSVM.

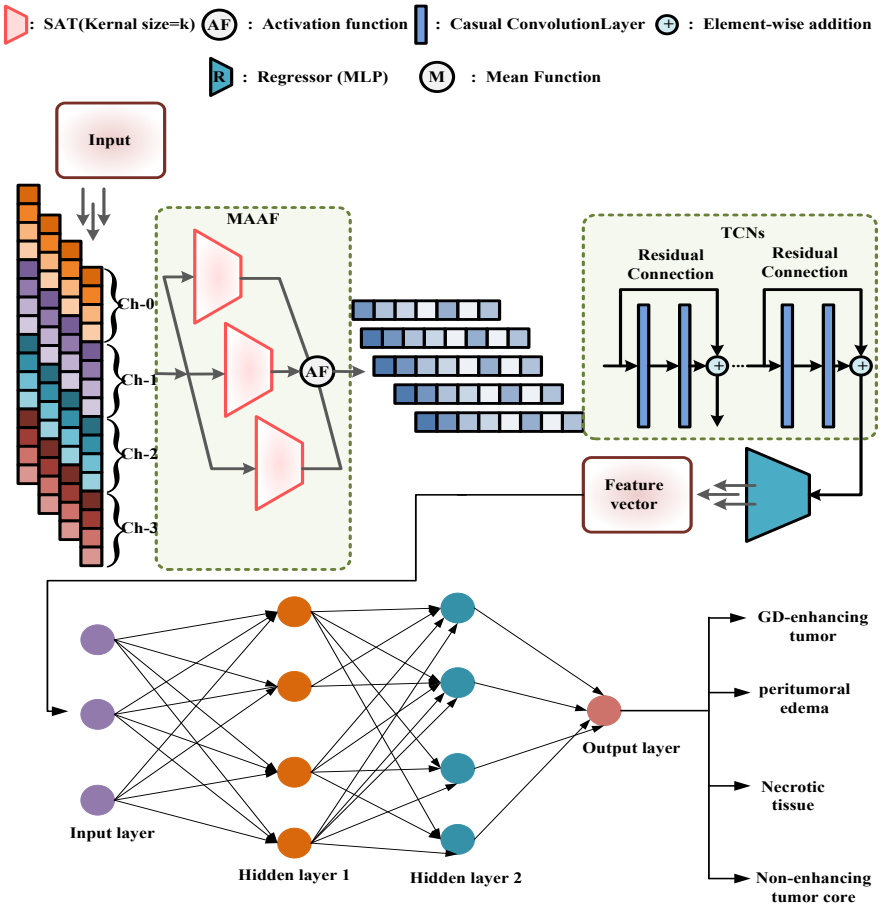

Figure 5: Architecture Diagram of MSTCNN-DSVM

A, Extraction of Intensity, Shape, and Texture Features utilizing Multi-Anchor Space-Aware Temporal Convolutional Neural Network

The MASTCNN [30] is used to extract Intensity-dependent Features, Shape-based Features, and Texture Features from MRI imageries. The pre-processed images are supplied to multi-anchor convolutional layers, which use kernels of varying sizes for capturing fine-grained local details and broader contextual features is given in equation (6).

$$u = \left[\left[q_{c0}^{f0},\ldots,q_{c0}^{f_{G-1}}\right],\ldots,\left[q_{cC-1}^{f0},\ldots,q_{cC-1}^{f_{G-1}}\right]\right] \quad (6)$$

Here, u represents the fine-grained local details; q denotes pre-processed images; f indicates the kernels of varying sizes; c denotes broader contextual features and C represents multi-anchor convolutional layers. The feature maps from the multi-anchor layers are processed by space-aware temporal layers, which analyze spatial relationships across different regions of the image over multiple contextual anchors. This step captures dynamic patterns and spatial dependencies as given in equation (7).

$$y = \left[u_0,\ldots,u_{t-1}\right] \quad (7)$$

Here, u indicates dynamic patterns and y represents spatial dependencies. The spatial-temporal features are then aggregated using pooling operations, like global average or max pooling, to decrease dimensionality while retaining the informative patterns. This step consolidates learned representations into a compact form is given in equation (8).

$$G(p) = G(p-1) + 2\times(l-1)\times e_p \quad (8)$$

Here, G represents the spatial-temporal features; p denotes informative patterns and e indicates pooling operations. Finally, the aggregated features are flattened to a one-dimensional feature vector. This vector encodes distinctive spatial and temporal characteristics of the tumor captured by MSTCNN is expressed in equation (9).

$$G(p) = 1 + 2\cdot(k-1)\cdot\sum_{i=0}^{p-1}2^i = 1 + 2\cdot(l-1)\cdot\left(2^p-1\right) \quad (9)$$

Here, k represents one-dimensional feature vector**.**

B, Classification utilizing Distributed Support Vector Machine

In this section, Classification utilizing Distributed Support Vector Machine [31] is discussed. Each distributed node receives its allocated subset of feature vectors extracted from the MASTCNN. A local Support Vector Machine is trained on this subset to identify the optimum hyper plane that separates the different MRI classes as given in equation (10).

$$K_m = K(x,c) \quad (10)$$

Where, K denotes optimal hyper plane, x denotes feature subset, c denotes different MRI classes .After local training, each node sends its learned parameters to a central coordinator node. This ensures that knowledge from all nodes contributes to a comprehensive understanding of the MRI feature space as expressed in equation (11).

$$\beta = \arg\{L(\beta)\} \quad (11)$$

Where, β denotes central coordinator node, L denotes MRI feature space. Central node aggregates the parameters from every local SVM to create a unified global model. Weighted averaging is used to combine local insights while minimizing bias as given in equation (12).

$$\beta^{k+1} = \arg\left\{\beta^k\right\} \quad (12)$$

The refined global Distributed SVM is utilized to categorize unseen MRI images depending on their feature vectors. Each input is evaluated against the learned hyper plane to assign class labels as evaluated in equation (13).

$$\alpha^k = \arg\left\{\min\left\{\alpha^k\right\}\right\} \quad (13)$$

Where, α denotes weighted averaging. Figure 6 shows Sample Images of Brain Tumour Categorization.

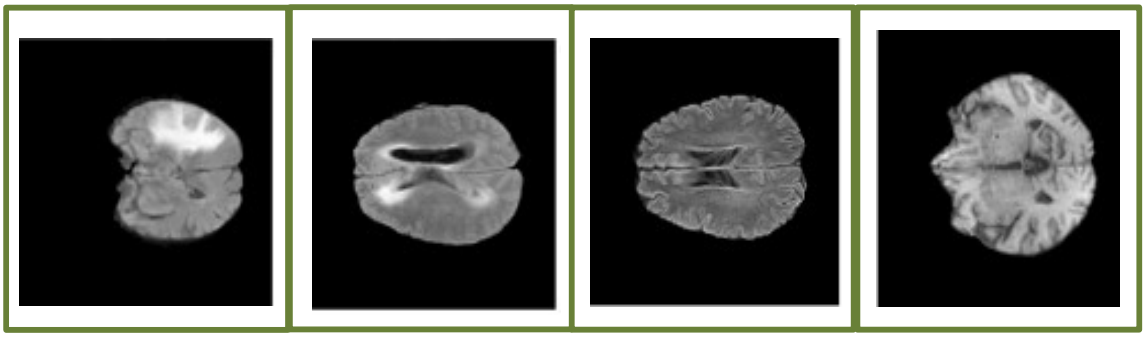

Figure 6: Sample Images of Brain Tumour Classification

Finally, MSTCNN-DSVM classifies the breast tumor as GD-enhancing tumor, peritumoral edema, necrotic tissue, non-enhancing tumor core based on input MRI images and feature vector.

3.4 Parameter Tuning with Super cell Thunderstorm Algorithm Metaheuristic

This section discusses the optimization using STA [32] to improve weight parameters $e_p and\ \beta^k$ of utilized MSTCNN-DSVM. The benefits of using the STA for optimizing weight parameters of used MSTCNN-DSVM are its ability to enhance detection accuracy, convergence speed and overall model robustness. STA uses the dynamic behavior of super cell storms to explore and utilize the solution space effectively, allowing it to escape local minima and discover optimal parameter configurations. These results in a more accurate classification of complex intrusion patterns, improved generalization to unseen data, and reduced false alarm rates. Its adaptive nature supports better fine-tuning of MSTCNN-DSVM parameters leading to a more dependable and energy-effectual intrusion detection system in WSN. The STA is inspired by the rare but powerful characteristics of super cell storms, known for their rotating updrafts, intense energy and severe impact. This dynamic and organized behavior is mimicked in the algorithm to achieve efficient exploration, fast convergence and optimal solutions in difficult optimization problems.Here, step by step procedure for acquiring regulates MSTCNN-DSVMutilizing STA is described. Each step technique is given below,

Step 1: Initialization

The STA approach simulates the activity of Super cell thunderstorms. The initial solutions are distributed uniformly across the search space expressed in equation (14).

$$Y_i = lb + r_i(ub - lb), i = 1,2,.....,n \tag{14}$$

Here, ub and lb are the lower as well as upper limits of search space, r_i represents arbitrary vector, this is evenly distributed in [0, 1]range and n denotes count of storm populace.

Step 2: Random Generation

Following setup, random factors were generated for the input. It is dependent upon an explicit hyper parameter requirement.

Step 3: Fitness Function

It creates random solution from initialization. It is measured using exploration node and determined by equation (15).

$$Fitness\ Function = Optimizing\ [e_p and\ \beta^k] \tag{15}$$

Here, the parameter e_p is employed to maximize the accuracy and W^{t-1} is employed to maximize the computational time.

Step 4: Spiral Motion for Optimizing e_p

Super cell thunderstorms have distinct rotation patterns and often resemble mesocyclones. This revolution is parallel to the spiralling motion seen in natural phenomena like storms and tornados. The STA simulates the spiral motion of a storm utilizing mathematical methods and approaches. The mathematical expression for this strategy is the provided equation (16).

$$Y_i(y+1) = \begin{cases} \alpha_1 \cdot \left(Y_{best}(y) + \sigma^2 - \beta_1 \cdot \left|Y_{best}(y) - e_p Y_i(y)\right|\right) + \alpha_2 \cdot Y_i(y), & if\ t_1 < \dfrac{y}{y_{\max}} \\ \alpha_1 \cdot \left(Y_{best}(y) + \beta_2 \cdot \left|Y_{best}(y) + \gamma_r - ZH_i(y)\right|\right) + \alpha_2 \cdot Y_i(y), & if\ t_1 < \dfrac{y}{y_{\max}} \end{cases} \tag{16}$$

Here, α_1 and α_2 implies the weight coefficients, which standardize the degree to which entities move towards optimal personage and earlier individual, $\gamma_r(i)$ represents the number of sentiment features respectively, e_p is the standard deviation of distances, y signifies the current iteration, $y_{\max}$ denotes the maximal count of iterations and $ZH_i(y)$ shows the mean group that is reached by taking into account the means of a set of randomly selected points that are near the solution candidate under consideration.

Step 5: Tornado Formation for Optimizing β^k

The most damaging characteristics of super cell thunderstorms are their capacity to generate tornadoes. Tornadoes are severe, violent windstorms that originate within a supercell's whirling updraft. STA aims for its algorithms to replicate the circumstances and mechanisms that guide to tornado configuration within supercells. By doing so, weather forecasters can more accurately forecast when and where tornadoes expand during a storm. Due to its significant impact on supercell thunderstorms, tornado formation has been carefully

considered in the model. To avoid falling into local optima, population positions are adjusted based on the dynamics of tornado formation. This level is accurately expressed as given in equation (17).

$$Y_i(y+1)=\begin{cases} Y_i(y)+\left[rand(0,1)\times\exp\left(-H_1\cdot\dfrac{y}{y_{\max}}\right)\right]\left(Y_{t3}(y)\beta^k-Y_{t4}(y)\right) \\ Y_i(y)+S+\left[YG(1-rand(0,1))+rand(0,1)\right]\left(Y_{t5}(y)-Y_{t6}(y)\right)\end{cases} \quad (17)$$

Where, β^k is the active adjacency matrix depending upon semantic similarity at time t, YG equals 0.7 and H_1 represents the step factor, t_2 denotes a random number while t_3, t_4, t_5, t_6 is the arbitrary indices of the storm. Algorithm 1 offers the pseudo code significant the STQ technique

Algorithm 1: Pseudo code of the STA technique

% STA setting
Determine the control parameter ($Dimension\ of\ problem(d)$*, maximum number of iterations, search agents), and parameter YG*
% Initialization
Initialize the populace arbitrarily
Assess the objective function of the novel solution
Attain the optimal solution
%Main Loop
While $y \le y_{\max}$
Update the $\alpha_1, \alpha_2, \beta_1$ *and* β_2 *using Equation (16).*
%Spiral Motion Stage
For *each population*
Update the location of by equation (16).
End for
%Create group
Assess the objective function of every individual
Obtain the optimal solution
%Tornado Formation stage
Update the H_1 *using equation (16).*
For *each population*
Update the location of by equation (17).
End For
% Create group
Verify the limits of the novel positions assess the objective function of each individual
Obtain the optimal solution
% Jetstream Phase
For each population
Update the location of utilizing equation (16)
End for
% Create group
Check the limits of the new positions assess the objective function of every individual
Obtain the optimal solution
$y = y + 1$
End while
Output the best solution

Step 6: Jet stream

A narrow, swift air movement in the high atmosphere is called a jet stream. It has a big impact on weather patterns and can affect how super cells and other violent thunderstorms originate and grow. Since the jet stream's interaction with a storm can substantially affect the storm's origin, evolution, and path, STA takes this factor into account. Storms prepare to strike the optimal location in the search region, causing all other points to converge towards it. This procedure is given in equation (18).

$$Y_i(y+1)=\begin{cases} rand\times Y_{best}(y)+f_1(o)\times\left(Y_i(y)-3\times rand\times Y_{mean}(y)\right) \\ \quad +x_1(i)\times\left(y_i-2\times Y_{berst}(y)\right)\ t_7\le 0.3 \\ Y_i(y)+rand\times\left[Y_{best}(y)-|Y_l(y)|\right]+rand\times\left[|Y_i(y)|-Y_l(y)\right]\ t_7>0.3 \end{cases} \quad (18)$$

Here, $x_1(i)$ represents the route of these storms throughout Jetstream motion, $Y_i(y)$ denotes product of variance among current, $Y_l(y)$ implies for mean points along polar $x-axis$ s and variance among present as well as optimum points along the polar $yaxis$.

Step 7: Termination

The weight parameter of generator $e_p and\ \beta^k$ from MSTCNN-DSVM is enhanced using STA otherwise repeat step 3 until satisfy halting criteria $Y=Y+1$ .Then; BTC-MSTCNN-DSVM-MRI assesses intrusion detection classification by increasing accuracy and reducing computational time.

4. Result and Discussion

The simulation outcomes of MSTCNN-DSVM method are deliberated in this sector. Proposed BTC-MSTCNN-DSVM-MRI method is simulated in Python on computer with 12GB RAM, Intel ®core (7M) i3-6100CPU @ 3.70GHz processor utilizing mentioned metrics. The count of iterations is equivalent to the number of batches needed to complete one epoch. The proposed BTC-MSTCNN-DSVM-MRI approach is evaluated to existing **BTC-GAN-MRI, BTD-MRI-DCNN** and **EffNetv2-MRI-BTC methods**.

4.1 Performance measures

Performance metrics like Accuracy, F1-score, Precision, recall, ROC and Computational Time are examined. These performance metrics are scaled under following matrices.

4.1.1 Accuracy

Accuracy calculates ratio of accurately categorized instances out of total instances. It reflects the overall exactness of the method in tumor type prediction. Higher accuracy indicates more reliable classification performance is determined by equation (19),

$$Accuracy=\frac{TP+TN}{TP+TN\ +FP+FN} \quad (19)$$

Where, TP represents true positive, TN signifies true Negative, FP represents false positive , FN represents false negative.

4.1.2 Precision

This metric measures the ratio of true positive predictions among every positive predictions created. It evaluates how accurately the model identifies a specific tumor class. Higher precision reduces false positive using equation (20).

$$\Pr ecision=\frac{TP}{TP+FP} \quad (20)$$

4.1.3 Recall

This metric calculates the ratio of true positive predictions between each actual positive instances. It assesses the methods capability to accurately identify every occurrences of a tumor type. Higher recall minimizes false negatives using equation (21),

$$\mathrm{Re}call=\frac{TP}{TP+FN} \quad (21)$$

4.1.4 F1-Score

This is the harmonic mean of precision and recall and provides a single measure of classification performance. It balances false positives including false negatives. Higher F1-score represents better overall prediction quality measured by equation (22),

$$F1-score=\frac{TP}{TP+FN} \quad (22)$$

4.1.6 Receiver Operating Characteristic

It refers true positive rate or sensitivity, versus false positive rate or 1-specificity and determined by equation (23)

$$ROC=0.5\times\left(\frac{TP}{TP+FN}+\frac{TN}{TN+FP}\right) \quad (23)$$

4.2 Training and Validation

Figure 7 and 8 shows training and validation of accuracy and loss. These plots highlight the model performance trends, emphasizing the need for potential regularization techniques to enhance validation accuracy and lessen overfitting.

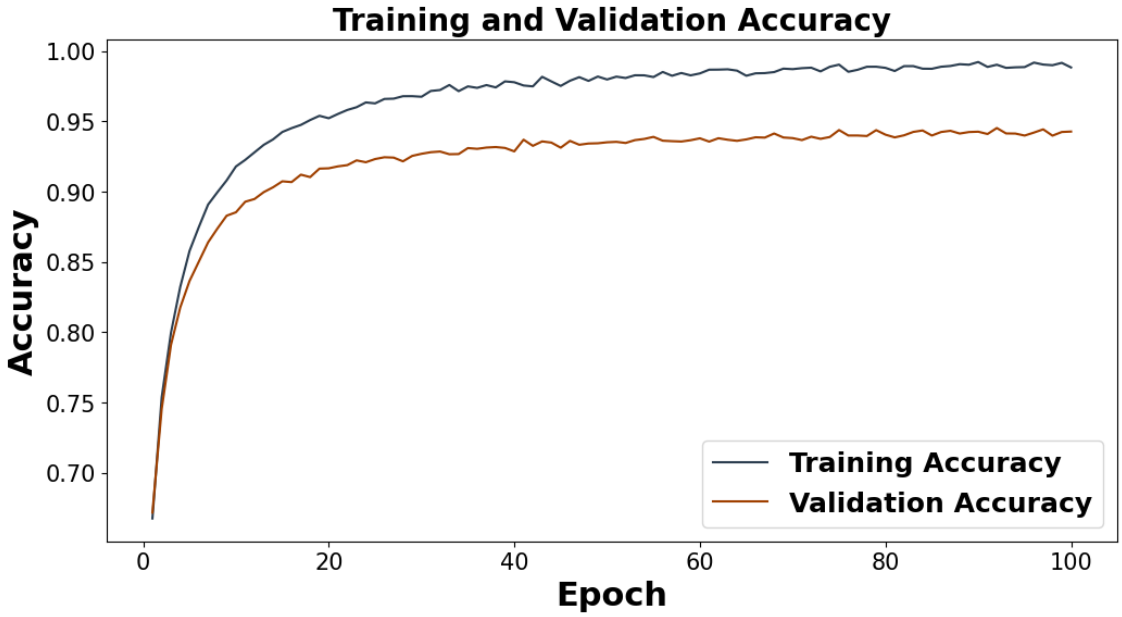

Figure 7: Training and Validation of Accuracy

Figure 7 indicates training and validation accuracy displayed on graph over a period of 100 epochs. Both accuracies progressively plateau after increasing steadily in the early stages. With a narrow generalization gap and high performance, the validation accuracy stabilizes at 94% and the training accuracy approaches nearly ninety percent. Although overall both metrics show that the model learns well and achieves high accuracy, this discrepancy signals slight overfitting due to the enhanced performance on training data compared to unknown validation data.

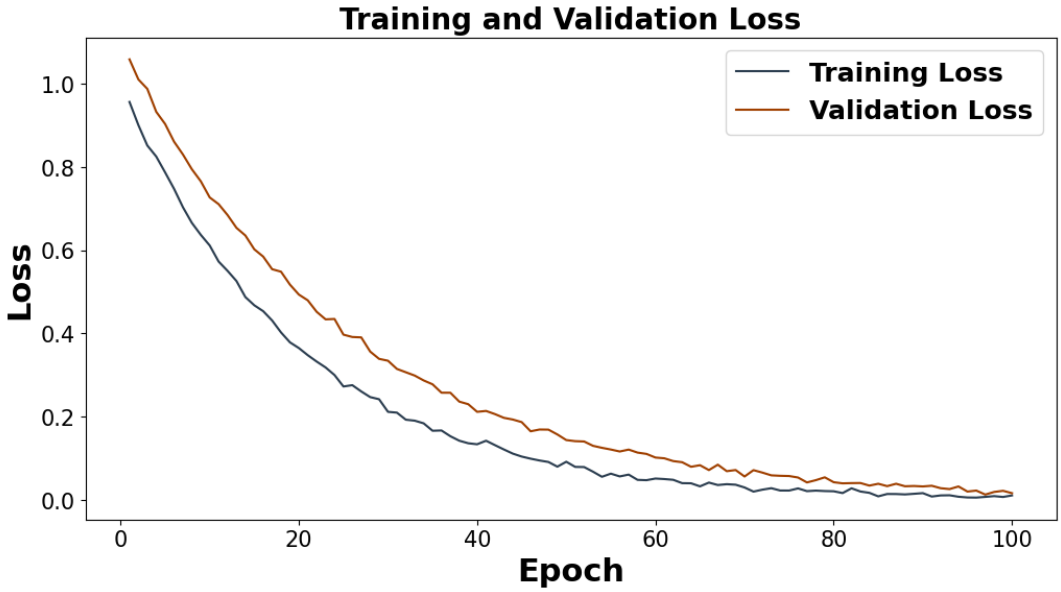

Figure 8: Training and Validation of Loss

Figure 8 represents training along validation losses are displayed on the graph over a period of 100 epochs. Both losses show a consistent decline and suggest that the model performing better. While the validation loss likewise exhibits a declining trend and stabilizes somewhat above the training loss, the training loss decreases more quickly and approaches zero. The model works well on training and unseen validation data, as indicated by tiny gap between the two curves, which indicates good generalization with low overfitting.

4.3 Performance Analysis

Table 3-5 and Figure 9-12 portrays simulation outcome of BTC-MSTCNN-DSVM approach. The proposed BTC-MSTCNN-DSVM is analyzed with existing BTC-GAN-MRI, BTD-MRI-DCNN and EffNetv2-MRI-BTC models.

Table 3: Accuracy analysis

Methods	Accuracy (%)			
	GD-Enhancing Tumor	Peritumoral Edema	Necrotic	Non-Enhancing Tumor Core
BTC-GAN-MRI	95.85	93.9	96.25	94.1
BTD-MRI-DCNN	92.8	93.25	91.95	96.85
EffNetv2-MRI-BTC	96.55	94.75	97.1	92.65
BTC-MSTCNN-DSVM-MRI(Proposed)	99.3	99.55	99.7	99.45

Table 3 depicts accuracy analysis. The proposed BTC-MSTCNN-DSVM-MRI technique achieves remarkably higher accuracy values of 99.3% for GD-Enhancing Tumor, 99.55% for Peritumoral Edema, 99.7% for Necrotic regions, and 99.45% for Non-Enhancing Tumor Core, compared to BTC-GAN-MRI's 95.85%, 93.9%, 96.25%, and 94.1%, BTD-MRI-DCNN's 92.8%, 93.25%, 91.95%, and 96.85%, and EffNetv2-MRI-BTC's 96.55%, 94.75%, 97.1%, and 92.65% respectively. This huge enhancement shows that integration of STA leads to better characterization of tumor sub-regions, which directly can aid in better planning of drug delivery and making of therapeutic decisions. These improvements in precision are essential to clinical MRI analysis, as they guarantee that subtypes of brain tumors are properly diagnosed with a minimal number of diagnostic errors, which, in the end, can be used to plan treatment and treat patients more effectively.

Table 4: Precision analysis

Methods	Precision (%)			
	GD-Enhancing Tumor	Peritumoral Edema	Necrotic	Non-Enhancing Tumor Core
BTC-GAN-MRI	93.55	94.85	95.4	93.2
BTD-MRI-DCNN	95.1	92.95	94.65	93.35
EffNetv2-MRI-BTC	94.25	96.1	92.8	95.55
BTC-MSTCNN-DSVM-MRI(Proposed)	98.55	98.2	98.75	98.45

Table 4 shows the precision analysis. The proposed BTC-MSTCNN-DSVM-MRI method also secures superior precision values of 98.55% for GD-Enhancing Tumor, 98.2% for Peritumoral Edema, 98.75% for Necrotic, and 98.45% for Non-Enhancing Tumor Core, outperforming BTC-GAN-MRI's 93.55%, 94.85%, 95.4%, and 93.2%, BTD-MRI-DCNN's 95.1%, 92.95%, 94.65%, and 93.35%, and EffNetv2-MRI-BTC's 94.25%, 96.1%, 92.8%, and 95.55%. These advances underline the fact that STA focuses on the decision boundaries by minimizing the false positives and learning the tumor-specific texture. The accuracy of brain tumor characterization to drug delivery and therapeutic planning helps to reduce the risk of the mislabeling of normal tissues as tumor regions and hence unnecessary medical procedures and provide an accurate radiological interpretation of the targeted treatment.

Table 5: Recall analysis

Methods	Recall (%)			
	GD-Enhancing Tumor	Peritumoral Edema	Necrotic	Non-Enhancing Tumor Core
BTC-GAN-MRI	93.1	95.25	92.95	94.8
BTD-MRI-DCNN	92.85	94.55	93.4	91.95
EffNetv2-MRI-BTC	95.05	92.7	96.15	93.35
BTC-MSTCNN-DSVM-MRI(Proposed)	98.4	98.75	98.2	98.65

Table 5 shows the recall analysis. The proposed BTC-MSTCNN-DSVM-MRI method further achieves higher recall values of 98.4% for GD-Enhancing Tumor, 98.75% for Peritumoral Edema, 98.2% for Necrotic, and 98.65% for Non-Enhancing Tumor Core, compared to BTC-GAN-MRI's 93.1%, 95.25%, 92.95%, and 94.8%, BTD-MRI-DCNN's 92.85%, 94.55%, 93.4%, and 91.95%, and EffNetv2-MRI-BTC's 95.05%, 92.7%, 96.15%, and 93.35%. The enhanced recall shows that STA enhances the capability of the methods to record

even minor variations of tumors and minimizes false negative. The ability to recall high in MRI-based tumor classification is vital since the absence of tumor tissues in the diagnosis may slow down the progress of treatment, therefore, the suggested approach will guarantee a more successful detection of malignant areas to enhance the prognosis.

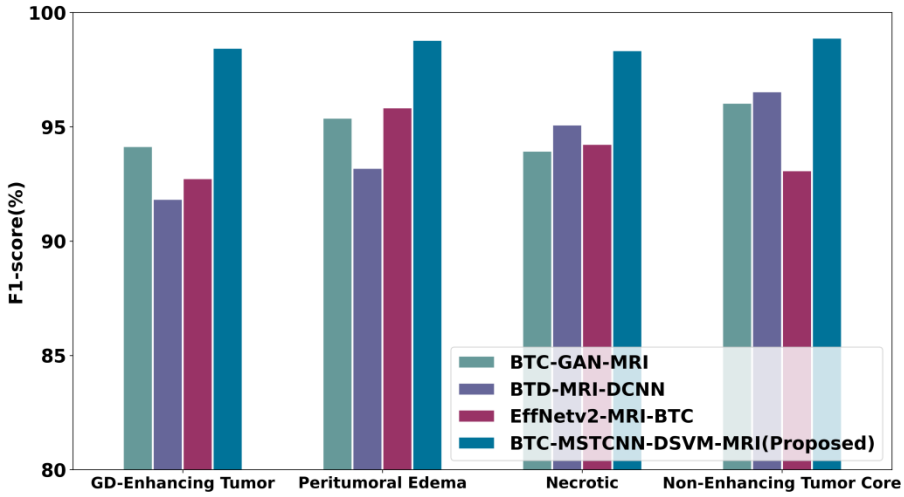

Figure 9: F1-score evaluation

Figure 9 indicates f1-score evaluation. The BTC-MSTCNN-DSVM-MRI method additionally records superior F1-scores of 98.45% for GD-Enhancing Tumor, 98.8% for Peritumoral Edema, 98.35% for Necrotic, and 98.9% for Non-Enhancing Tumor Core, while BTC-GAN-MRI achieved 94.15%, 95.4%, 93.95%, and 96.05%, BTD-MRI-DCNN obtained 91.85%, 93.2%, 95.1%, and 96.55%, and EffNetv2-MRI-BTC delivered 92.75%, 95.85%, 94.25%, and 93.1%. The resolution of the balance between high precision and recall is proved by the enhanced F1-scores, which point to the strength of STA to meet the challenge of tumor boundary complexity and overlapping tissue appearance. In medical imaging, the larger the F1-score, the better the detection and reduced diagnostic uncertainty, which gives a better basis on clinical decision-making in brain tumor treatment strategies.

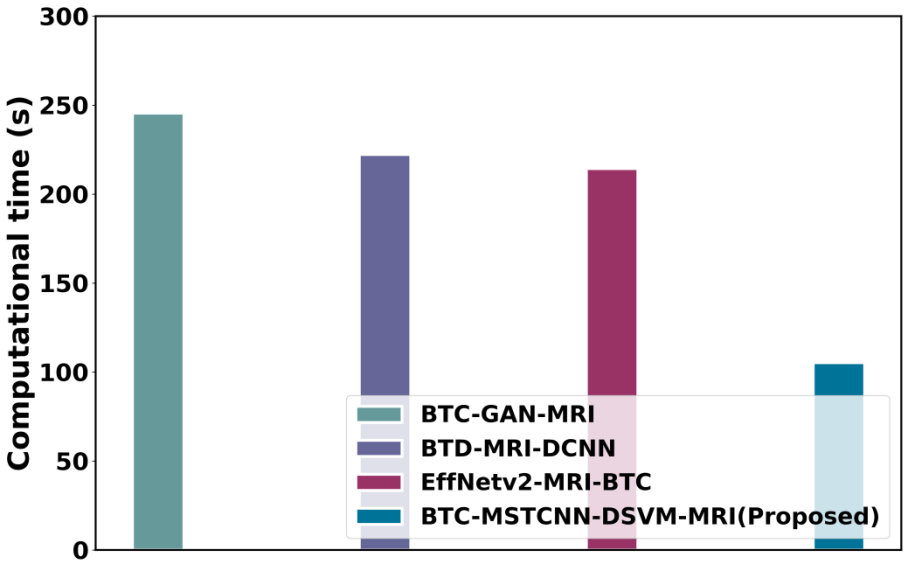

Figure 10: Computational time analysis

Figure 10 indicates computational time analysis. The BTC-MSTCNN-DSVM-MRI method also significantly reduces computational time to 105.2 seconds, compared to BTC-GAN-MRI's 245.58 seconds, BTD-MRI-DCNN 222.22 seconds, and EffNetv2-MRI-BTC's 214.4 seconds. This notable reduction results from the optimized design of the MSTCNN, which enables efficient temporal feature learning, reduces redundant computations, and accelerates the extraction of higher level tumor features from MRI scans. Faster computational time is highly beneficial in medical environments where real-time or near real-time analysis

is required, allowing radiologists to obtain quick and reliable tumor classification results without compromising diagnostic accuracy.

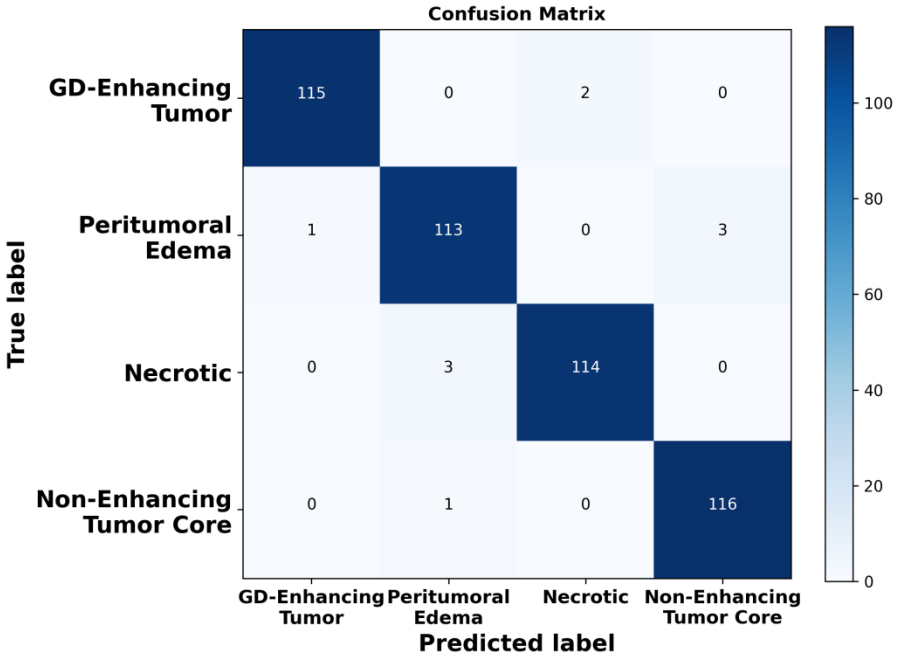

Figure 11: Confusion Matrix for tumor tissue classification

Figure 11 represents the confusion matrix for tumor tissue classification across four mentioned categories. The diagonal entries represent correct classifications, showing high accuracy with 115 GD-Enhancing Tumor, 113 Peritumoral Edema, 114 Necrotic, 116 Non-Enhancing Tumor Core samples correctly identified. Misclassifications are minimal, like 2 GD-Enhancing Tumor misclassified as Necrotic, 1 Peritumoral Edema misclassified as GD-Enhancing Tumor, 3 Peritumoral Edema misclassified as Non-Enhancing Tumor Core, 3 Necrotic misclassified as Peritumoral Edema, 1 Non-Enhancing Tumor Core misclassified as Peritumoral Edema. The distribution shows strong model performance with very low off-diagonal values, indicating precise distinction between tumor subtypes and minimal overlap in prediction errors, thereby confirming robustness and reliability of the classification framework.

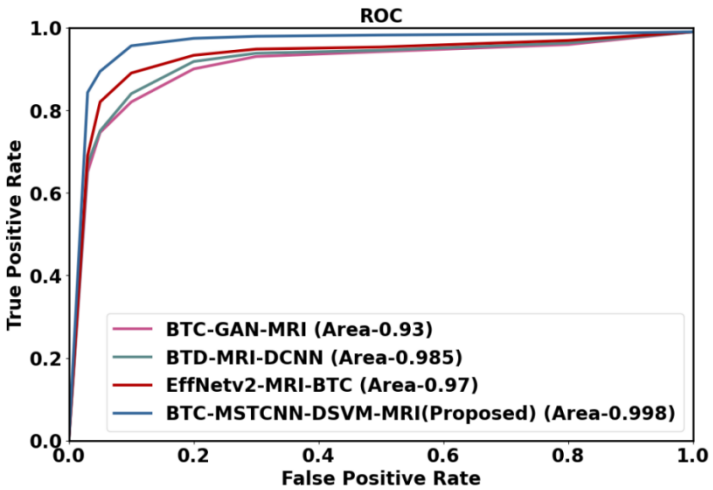

Figure 12:Receiver Operating Characteristic

Figure 12 shows the ROC curve compares the performance of four different brain tumor characterization for drug delivery and therapeutic planning models in distinguishing true positives from false positives. The proposed BTC-MSTCNN-DSVM-MRI model achieves the greatest ROC of 0.998, representing superior sensitivity and specificity evaluated to BTC-GAN-MRI (0.93), BTD-MRI-DCNN (0.985), and EffNetv2-MRI-BTC (0.97). The step rise of the BTC-MSTCNN-DSVM-MRI curve at low false

positive rates demonstrates its strong capability to accurately detect tumor regions with minimal misclassification, highlighting its robustness and reliability for accurate MRI-based tumor detection.

4.4 Computational Complexity

The computational complexity of Super cell Thunderstorm Algorithm primarily based upon spatial and temporal resolution of meteorological data, the number of grid points, and the iterative calculations required for storm identification, tracking, and classification. The algorithm involves Preprocessing radar reflectivity and velocity fields, feature extraction for storm cores and mesocyclones, and continuous updating through time steps. Typically, the complexity can be expressed as $O(N \times T)$,here N denotes count of spatial grid points analyzed , T implies number of temporal iterations. Additional complexity arises from feature correlation, vertical wind shear analysis, and clustering operations for storm structure classification, which may scale up to $O(N \log N)$ for sorting-based segmentation or $O(N^2)$ for pairwise spatial correlation. Overall, the algorithm is computationally intensive but manageable with parallel processing and optimized data handling. Figure 7 shows the computational complexity.

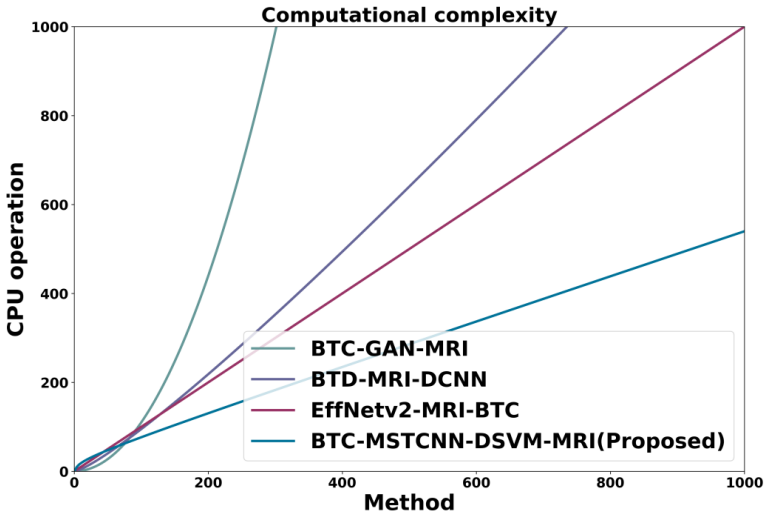

Figure 13: Computational Complexity

Figure 13 illustrates the computational complexity comparison of different MRI-based methods in terms of CPU operations with respect to the number of methods applied. The graph shows that BTC-GAN-MRI demonstrates the steepest curve, indicating significantly higher computational demand as the method size increases. BTD-MRI-DCNN and EffNetv2-MRI-BTC also exhibit high computational growth, with EffNetv2-MRI-BTC being moderately lower than BTD-MRI-DCNN but still rising steeply. In contrast, the proposed BTC-MSTCNN-DSVM-MRI method achieves the lowest computational complexity, maintaining a comparatively gradual increase in CPU operations even as the method scale grows, thus proving its efficiency and scalability over the existing approaches.

4.5 Statistical Comparison

The statistical comparison of the proposed BTC-MSTCNN-DSVM-MRI method with existing approaches, namely BTC-GAN-MRI, BTD-MRI-DCNN, and EffNetv2-MRI-BTC, is presented in Table 10. This evaluation considers multiple performance indicators, and P-values determine the statistical significance of improvements, the BTC-MSTCNN-DSVM-MRI method consistently outperforms the existing techniques across all metrics, achieving greater accuracy, precision, recall, F1-score, with extensively reduced computational time. These outcomes confirm the effectiveness and robustness of the BTC-MSTCNN-DSVM-MRI method in BT categorization.

Table 6: Statistical Comparison of the Proposed Method (BTC-MSTCNN-DSVM-MRI) vs Existing Methods

Metric	BTC-MSTCNN-DSVM-MRI (Proposed)	BTC-GAN-MRI	BTD-MRI-DCNN	EffNetv2-MRI-BTC	P-value (Proposed vs Existing)
Accuracy (%)	99.3	95.85	92.8	96.55	0.001
Precision (%)	98.55	93.55	95.1	94.25	0.002
Recall (%)	98.4	93.1	92.85	95.05	0.003
F1-Score (%)	98.45	94.15	91.85	92.75	0.002

Computational Time (s)	105.2	245.58	222.22	214.4	0.001

Table 6 represents a comprehensive statistical comparison of the BTC-MSTCNN-DSVM-MRI framework against existing methods including BTC-GAN-MRI, BTD-MRI-DCNN, and EffNetv2-MRI-BTC across key performance indicators. The BTC-MSTCNN-DSVM-MRI model attains greater accuracy of 99.3%, significantly outperforming existing approaches, which range between 92.8% and 96.55%. Similarly, it records superior precision (98.55%), recall (98.4%), F1-score (98.45%), highlighting its balanced

capability in detecting true tumor regions while minimizing false predictions. In addition, the computational time of BTC-MSTCNN-DSVM-MRI model is drastically reduced to 105.2 seconds, compared to 214.4–245.58 seconds for other techniques, emphasizing its efficiency. The consistent improvements across all metrics indicate that the BTC-MSTCNN-DSVM-MRI technique not only enhances diagnostic accuracy also ensures robustness and faster processing, making it more suitable for clinical deployment compared to existing brain tumor categorization techniques.

4.6 Discussion

The findings reveal that the proposed **BTC-MSTCNN-DSVM-MRI** framework is a highly effective approach for precise brain tumor detection and categorization from MRI imageries. Extensive evaluations using performance measures like Accuracy, Precision, Recall, F1-Score, Computational Time, Computational Complexity, and confusion matrix confirm that the proposed method substantially outperforms existing models including **BTC-GAN-MRI, BTD-MRI-DCNN,** and **EffNetv2-MRI-BTC**. Built on BRATS 2020 dataset, the proposed approach integrates pre-processing with **SMSVSF** for enhanced image quality, followed by augmentation to enrich data diversity, and multi-feature extraction using **MSTCNN**. The extracted intensity, shape, texture features are then classified by **DSVM** into GD-enhancing tumor, peritumoral edema, necrotic tissue, non-enhancing tumor core, while **STA optimization** refines the model parameters to maximize classification precision and reduce computational burden. The proposed method achieves superior precision and recall compared to existing techniques with 99.55% accuracy offering a more reliable and efficient diagnostic solution. In addition to accuracy of classification, the methodology can be used to facilitate optimal decisions in drug delivery, individualized chemotherapy, and prompt pharmacological interventions. Pharmaceutical science-wise, the proposed framework can be viewed as a decision-support system that assists the clinician in changing the approach to drug delivery depending on the heterogeneity of the tumor. This helps in increased therapeutic efficacy, decreased systemic toxicity, and patient specific treatment outcomes.

5. Conclusion

In this section, BTC-MSTCNN-DSVM-MRI was successfully implemented. BTC-MSTCNN-DSVM-MRI method is executed the presentation of proposed. According to the experimental results BTC-MSTCNN-DSVM-MRI performed better when utilized with Co-training technique than when used separately regards accuracy, precision. The BTC-MSTCNN-DSVM-MRI approach attains 99.55% higher accuracy, 98.75% higher precision and 98.65% higher recallwhen analyzed with existing methods BTC-GAN-MRI, BTD-MRI-DCNN and EffNetv2-MRI-BTC. A limitation is the reliance on a single publicly available dataset, which limits generalizability to other clinical settings. Another problem is dealing with highly imbalanced data distributions, as even rare tumor types might be misclassified despite great overall accuracy. As well, real-time clinical deployment may confront limits in terms of computer resources, scalability, and integration with existing medical imaging systems. The next step in work will be the combination of pharmacokinetic and pharmacodynamic modeling, prediction of drug responses, and explainable AI methods to optimize drug delivery and individual therapy planning further. Interactive approaches to multimodal medical data, such as the genetic information, pathology, imaging information could enhance classification precision and personalized planning of therapy. Moreover, the implementation of AI-assisted diagnostic tools in real-time in the healthcare setting facilitates the early intervention and constant monitoring of patients, which results in improved survival outcomes.

REFERENCE

1. Sandhiya, B. and Raja, S.K.S., 2024. Deep learning and optimized learning machine for brain tumor classification. Biomedical Signal Processing and Control, 89, p.105778.
2. Mohanty, B.C., Subudhi, P.K., Dash, R. and Mohanty, B., 2024. Feature-enhanced deep learning technique with soft attention for MRI-based brain tumor classification. International Journal of Information Technology, 16(3), pp.1617-1626.
3. Priya, A. and Vasudevan, V., 2024. Brain tumor classification and detection via hybrid alexnet-gru based on deep learning. Biomedical Signal Processing and Control, 89, p.105716.
4. Prasad, V., S, V. and B, S.R., 2024. K-Net-Deep joint segmentation with Taylor driving training optimization based deep learning for brain tumor classification using MRI. The Imaging Science Journal, 72(4), pp.499-519.
5. İncir, R. and Bozkurt, F., 2024. Improving brain tumor classification with combined convolutional neural networks and transfer learning. Knowledge-Based Systems,

299, p.111981.
6. Geetha, M., Srinadh, V., Janet, J. and Sumathi, S., 2024. Hybrid archimedes sine cosine optimization enabled deep learning for multilevel brain tumor classification using mri images. Biomedical Signal Processing and Control, 87, p.105419.
7. AG, B., Srinivasan, S., P, M., Mathivanan, S.K. and Shah, M.A., 2024. Robust brain tumor classification by fusion of deep learning and channel-wise attention mode approach. BMC Medical Imaging, 24(1), p.147.
8. Solanki, S., Singh, U.P., Chouhan, S.S. and Jain, S., 2024. A systematic analysis of magnetic resonance images and deep learning methods used for diagnosis of brain tumor. Multimedia Tools and Applications, 83(8), pp.23929-23966.
9. Sharif, M.I., Li, J.P., Khan, M.A., Kadry, S. and Tariq, U., 2024. M3BTCNet: multi model brain tumor classification using metaheuristic deep neural network features optimization. Neural Computing and Applications, 36(1), pp.95-110.
10. Almufareh, M.F., Imran, M., Khan, A., Humayun, M. and Asim, M., 2024. Automated brain tumor segmentation and classification in MRI using YOLO-based deep learning. IEEE Access, 12, pp.16189-16207.
11. Ramakrishnan, A.B., Sridevi, M., Vasudevan, S.K., Manikandan, R. and Gandomi, A.H., 2024. Optimizing brain tumor classification with hybrid CNN architecture: Balancing accuracy and efficiency through oneAPI optimization. Informatics in Medicine Unlocked, 44, p.101436.
12. Subba, A.B. and Sunaniya, A.K., 2025. Computationally optimized brain tumor classification using attention based GoogLeNet-style CNN. Expert Systems with Applications, 260, p.125443.
13. Rajput, I.S., Gupta, A., Jain, V. and Tyagi, S., 2024. A transfer learning-based brain tumor classification using magnetic resonance images. Multimedia Tools and Applications, 83(7), pp.20487-20506.
14. Khan, S.U.R., Zhao, M., Asif, S. and Chen, X., 2024. Hybrid-NET: a fusion of DenseNet169 and advanced machine learning classifiers for enhanced brain tumor diagnosis. International Journal of Imaging Systems and Technology, 34(1), p.e22975.
15. Ahsan, R., Shahzadi, I., Najeeb, F. and Omer, H., 2025. Brain tumor detection and segmentation using deep learning. Magnetic Resonance Materials in Physics, Biology and Medicine, 38(1), pp.13-22.
16. Turk, O., Ozhan, D., Acar, E., Akinci, T.C. and Yilmaz, M., 2024. Automatic detection of brain tumors with the aid of ensemble deep learning architectures and class activation map indicators by employing magnetic resonance images. ZeitschriftfürMedizinischePhysik, 34(2), pp.278-290
17. Batool, A. and Byun, Y.C., 2025. A Lightweight multi-path convolutional neural network architecture using optimal features selection for multiclass classification of brain tumor using magnetic resonance images. Results in Engineering, p.104327
18. Mandloi, S., Zuber, M. and Gupta, R.K., 2024. An explainable brain tumor detection and classification model using deep learning and layer-wise relevance propagation. Multimedia Tools and Applications, 83(11), pp.33753-33783.
19. Cekic, E., Pinar, E., Pinar, M. and Dagcinar, A., 2024. Deep learning-assisted segmentation and classification of brain tumor types on magnetic resonance and surgical microscope images. World Neurosurgery, 182, pp.e196-e204
20. Sultanpure, K.A., Bagade, J., Bangare, S.L., Bangare, M.L., Bamane, K.D. and Patankar, A.J., 2024. Internet of things and deep learning based digital twins for diagnosis of brain tumor by analyzing MRI images. Measurement: Sensors, 33, p.101220.
21. Yurtsever, M.E., Atay, Y., Arslan, B. and Sagiroglu, S., 2024. Development of brain tumor radiogenomic classification using GAN-based augmentation of MRI slices in the newly released gazi brains dataset. BMC Medical Informatics and Decision Making, 24(1), p.285.
22. Preetha, R., Priyadarsini, M.J.P. and Nisha, J.S., 2024. Automated Brain Tumor Detection from Magnetic Resonance Images Using Fine-Tuned EfficientNet-B4 Convolutional Neural Network. IEEE Access.
23. Pacal, I., Celik, O., Bayram, B. and Cunha, A., 2024. Enhancing EfficientNetv2 with global and efficient channel attention mechanisms for accurate MRI-Based brain tumor classification. Cluster Computing, 27(8), pp.11187-11212.
24. Nassar, S.E., Yasser, I., Amer, H.M. and Mohamed, M.A., 2024. A robust MRI-based brain tumor classification via a hybrid deep learning technique. The Journal of Supercomputing, 80(2), pp.2403-2427.
25. Joshi, A.A. and Aziz, R.M., 2024. Deep learning approach for brain tumor classification using metaheuristic optimization with gene expression data. International Journal of Imaging Systems and Technology, 34(2), p.e23007.
26. Simo, A.M.D., Kouanou, A.T., Monthe, V., Nana, M.K. and Lonla, B.M., 2024. Introducing a deep learning method for brain tumor classification using MRI data towards better performance. Informatics in Medicine Unlocked, 44, p.101423.
27. Malakouti, S.M., Menhaj, M.B. and Suratgar, A.A., 2024. Machine learning and transfer learning

techniques for accurate brain tumor classification. Clinical eHealth, 7, pp.106-119.
28. https://www.kaggle.com/datasets/awsaf49/brats20-dataset-training-validation
29. Piavanini, M., Brambilla, M. and Nicoli, M., 2025. Switching Model Stein Variational Sampling Filter for Mixed LOS/NLOS Industrial Indoor Positioning. IEEE Journal of Indoor and Seamless Positioning and Navigation
30. Sivabalan, S. and Minu, R.I., 2025. Optimized multi-anchor space-aware temporal convolutional neural network for automobile sales prediction.Knowledge-Based Systems, 311, p.113000.
31. Navia-Vazquez, A., Gutierrez-Gonzalez, D., Parrado-Hernández, E. and Navarro-Abellan, J.J., 2024. Distributed support vector machines. IEEE Transactions on Neural Networks, 17(4), pp.1091-1097.
32. Hassan, M.H. and Kamel, S., 2025. Supercell thunderstorm algorithm (STA): a nature-inspired metaheuristic algorithm for engineering optimization. Neural Computing and Applications, 37(10), pp.7207-7260